crystals

MDPI

Article

Impact of Long-Term Annealing on Photoluminescence from $Ge_{1-x}Sn_x$ Alloys

Oluwatobi Olorunsola [1,2], Hryhorii Stanchu [2,3], Solomon Ojo [1,4], Krishna Pandey [4], Abdulla Said [4], Joe Margetis [5], John Tolle [5], Andrian Kuchuk [3], Yuriy I. Mazur [3], Gregory Salamo [3,6,*] and Shui-Qing Yu [1,3]

1 Department of Electrical Engineering, University of Arkansas, Fayetteville, AR 72701, USA; ogolorun@uark.edu (O.O.); soojo@uark.edu (S.O.); syu@uark.edu (S.-Q.Y.)
2 Microelectronics-Photonics Program, University of Arkansas, Fayetteville, AR 72701, USA; hstanchu@uark.edu
3 Institute for Nanoscience and Engineering, University of Arkansas, Fayetteville, AR 72701, USA; kuchuk@uark.edu (A.K.); ymazur@uark.edu (Y.I.M.)
4 Material Science and Engineering Program, University of Arkansas, Fayetteville, AR 72701, USA; kpandey@uark.edu (K.P.); asa051@uark.edu (A.S.)
5 School of Electrical, Energy and Computer Engineering, Arizona State University, Tempe, AZ 85287, USA; joe.margetis@gmail.com (J.M.); john.tolle@cox.net (J.T.)
6 Department of Physics, University of Arkansas, Fayetteville, AR 72701, USA
* Correspondence: salamo@uark.edu

Abstract: We report on the connection between strain, composition, defect density and the photoluminescence observed before and after annealing at 300 °C for GeSn samples with Sn content of 8% to 10%. Results show how the composition and level of strain influenced the separation between the indirect and direct optical transitions, while changes in the level of strain also influenced the density of misfit dislocations and surface roughness. The effect of annealing is observed to lower the level of strain, decreasing the energy separation between the indirect and direct optical transitions, while also simultaneously increasing the density of misfit/threading dislocations and surface roughness. The reduction in energy separation leads to an increase of photoluminescence (PL) emission, while the increase of misfit/threading dislocations density and surface roughness results in a decrease of PL. Consequently, the competition between these factors is observed to determine the impact of annealing on the PL. As a result, annealing increases the collected PL for small (≤40 meV) separation between the indirect to direct optical transitions in the as-grown sample while decreases the PL for larger (≥60 meV) separations. More generally, these numbers have a small dependence on the level of strain in the as-grown samples.

Keywords: germanium tin; annealing; direct and indirect optical transition; strain engineering

Citation: Olorunsola, O.; Stanchu, H.; Ojo, S.; Pandey, K.; Said, A.; Margetis, J.; Tolle, J.; Kuchuk, A.; Mazur, Y.I.; Salamo, G.; et al. Impact of Long-Term Annealing on Photoluminescence from $Ge_{1-x}Sn_x$ Alloys. *Crystals* **2021**, *11*, 905. https://doi.org/10.3390/cryst11080905

Academic Editor: Chang Seop Hong

Received: 14 July 2021
Accepted: 30 July 2021
Published: 31 July 2021

1. Introduction

Recent research on group IV semiconductors has pointed to the potential of GeSn alloys for significant optoelectronic and photonic devices [1,2]. A special feature of the group-IV bi-alloy system, as in the case of Ge_xSn_{1-x}, is the unique capability to tune the Sn composition in the Ge matrix to achieve a lattice constant and/or bandgap to meet specific needs of photonic devices, from light emitters [3], to laser diodes [4] and to photodetectors [5]. Perhaps even more attractive is the feature that GeSn devices can be monolithically integrated on a Si platform through a standard complementary metal oxide (CMOS) process. This creates the opportunity to integrate photonic and electronic devices on a single Si substrate with optical capability in the needed near to mid-infrared [3,6,7] range. This is possible because, while Ge has an indirect bandgap, adding α-Sn results in the semiconductor GeSn, which transitions from an indirect to direct bandgap semiconductor with increasing Sn composition. For example, theoretical bandgap modelling efforts have predicted GeSn to transition from a Ge indirect bandgap to a direct bandgap with

Sn incorporation in the 7–12% [8–10] range. Adding Sn reduces the energy separation between the indirect L-valley and the direct Γ-valley until the energy difference goes to zero and then reverses sign. Interestingly, the optical properties of GeSn samples, with a composition near the transition point, are very sensitive to changes in composition or strain. On the experimentally side, despite the low-equilibrium solid solubility of Sn in Ge of only 1% [11], growth under compressive strain of high Sn concentrations has been achieved, demonstrating the indirect-to-direct transition [12–14] and fabrication of direct bandgap GeSn devices with high optical emission efficiency [15–18]. However, how much Sn can be achieved in GeSn and how stable GeSn with high Sn content can be at operating temperatures above room temperature, must be investigated.

For example, Du et al. [15] investigated GeSn with sufficient Sn content to observe the competition between indirect and direct optical transitions. The results confirm progressive enhancement of the direct transition over the indirect transition with increasing Sn composition. Meanwhile, Harris et al. [16] investigated photoluminescence (PL) at different temperatures from unstrained $Ge_{1-x}Sn_x$, to uncover that the indirect-to-direct transition occurs at a Sn concentration of about 6.7%. In fact, the role of strain is made very clear in a comprehensive study of optical transitions in $Ge_{0.875}Sn_{0.125}$ via PL measurements as a function of temperature, compressive strain and excitation power [17]. Complementing these studies, Stanchu et al. [18] recently demonstrated a correlation between strain relief, misfit dislocations, and Sn out-diffusion in thermally annealed GeSn at 300 °C. Together, these studies point out the possible existence of a strong connection between (1) strain, (2) composition, (3) defect density and (4) the performance of GeSn optical devices operating at temperatures, at and above, room temperature.

In this paper, we will examine the competition between the indirect and direct optical transition, at temperatures above room temperature, for as-deposited and annealed at 300 °C GeSn samples with Sn concentrations of 8% to 10%. Our objectives are to identify: (1) the connection between strain, composition, defect density and the PL observed before and after annealing, and (2) how the level of strain in as-grown samples can extend device performance, and even improve performance, by annealing at temperatures up to 300 °C.

2. Materials and Methods

For this study, GeSn samples with 8% to 10% Sn composition were grown in an ASM Epsilon®reduced pressure chemical vapor deposition (RPCVD) machine (ASM America, Inc, Phoenix, Arizona, USA). Thick Ge-buffer films (~700 nm) were initially grown on a hydrogen-passivated Si(001)-substrate using GeH_4 precursor. The Ge buffer layer deposition was followed by the growth of the GeSn layer by introducing the GeH_4 and $SnCl_4$ precursors into the chamber. The GeSn layers of samples S14 and S29 were grown at 310 °C and that of samples S15 and S32 were grown at 300 °C for CMOS compatibility. Control of the level of strain in the as-grown samples was achieved by a combination of growth-dependent parameters, such as, thickness, temperature, and growth rate. To examine the connection between strain, composition, defect density, and PL performance at elevated temperatures, we specifically investigated the impact of annealing treatments on the optical transition strength of four different GeSn samples, S14, S15, S29 and S32, each grown by RPCVD on a Ge (001) buffer on a Si (001) substrate. It should be noted that while the Sn content in the GeSn layer of samples S14 and S15 is uniform, the GeSn layer of samples S29 and S32 display spontaneously formed bottom and top regions with slightly different Sn content, which formed in result of strain relaxation. The structural parameters of samples S14, S15, S29, and S32 are compared in Table S2 of the Supplementary Material section.

For the annealing experiments, four small samples were taken from the center of the S14, S15, S29, and S32 4-inch diameter as-grown wafer. In each case, one of the four samples was designated as the "as-grown" unannealed sample. The other three samples were subjected to thermal treatments at 300 °C in vacuum for 2, 4, and 8 h, respectively. X-ray diffraction (Panalytical X'pert Pro MRD diffractometer) (Panalytical, Amsterdam, Netherlands)measurements (Figure 1), including reciprocal space maps (RSMs) (Figure 2),

coupled with modeling [18], were used to determine the lattice constants, Sn compositions, strain parameters, and misfit dislocations, of the annealed and unannealed samples.

Optical measurements were also taken for each sample using a standardized off-axis arrangement and lock-in detection technique, including a spectrometer connected to an InSb detector with a cut-off response of 3.0 µm, to capture the PL peaks and study the competition between the indirect and direct bandgap transitions. Two different excitation laser wavelengths (Table 1) were used to probe the PL emission from the samples: a 532 nm continuous wave (CW) and a 1064 nm pulsed laser (repetition rate of 45 kHz and pulse width of 5 ns). The two different laser wavelengths allowed samples with different thicknesses to be probed due to the different optical penetration depth for 532 nm and 1064 nm light [19]. The samples were enclosed in a helium-cooled cryostat, and the temperature was varied from 10 K to 300 K to obtain and systematically analyze temperature-dependent PL intensities. The temperature-dependent PL intensities were useful to identify which of the observed PL peaks corresponded to the indirect and direct optical transitions.

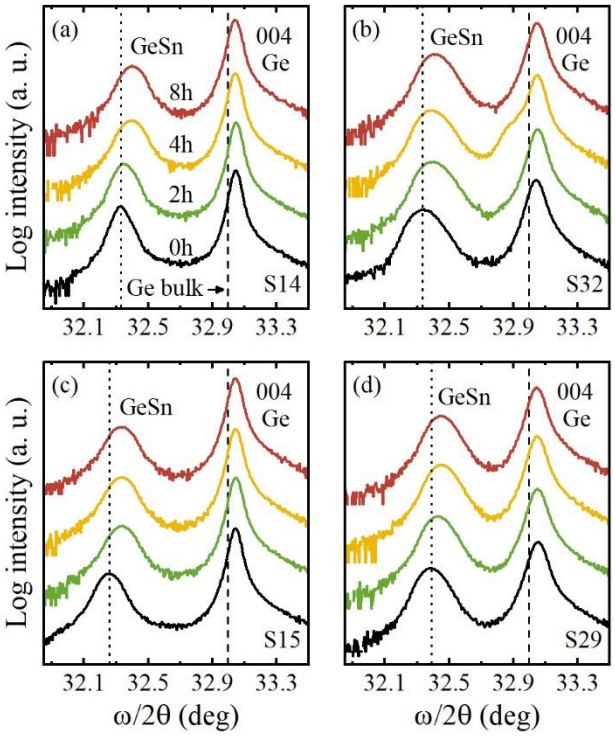

Figure 1. X-ray diffraction 004 $\omega/2\theta$ scans for samples (**a**) S14, (**c**) S15, (**d**) S29, and (**b**) S32 showing not much change in composition. The vertical dotted and dashed lines mark the peak positions of the as-grown GeSn and bulk Ge, respectively.

Table 1. Summarized laser pumping parameters.

Laser Wavelength (nm)	Spot Diameter (µm)	Average Power (mW)	Average Power Density (kW/cm^2)	Excitation Carrier Density (Photon/s/cm^2)	Penetration Depth (nm)
532	64	500	15	4.1×10^{19}	~100
1064	51	300	6	3.5×10^{22}	~900

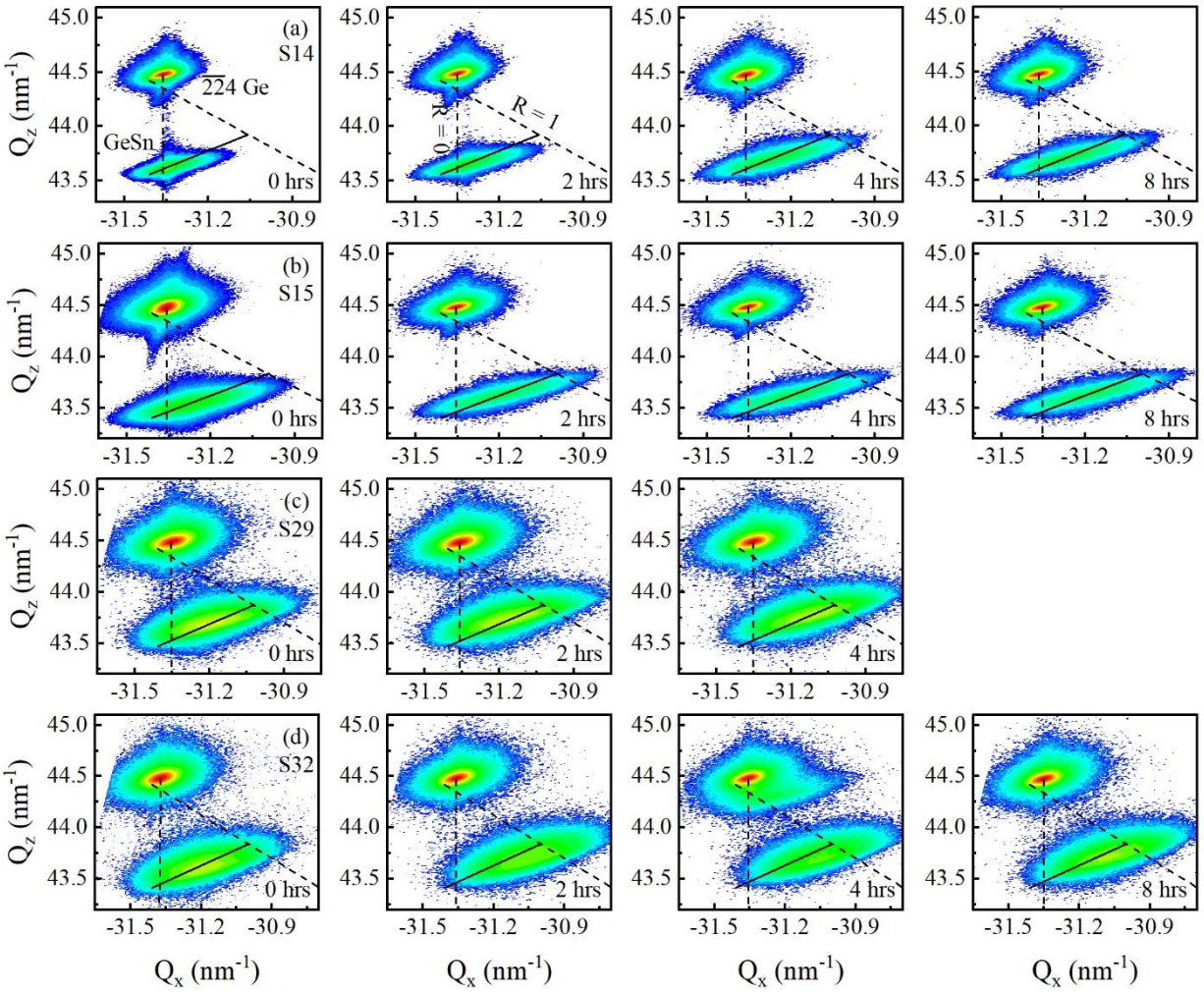

Figure 2. X-ray diffraction $\overline{2}24$ RSMs for samples (**a**) S14, (**b**) S15, (**c**) S29, and (**d**) S32 measured after the annealing for 0, 2, 4, and 8 h. The vertical and inclined dashed lines mark the fully strained and fully relaxed GeSn alloy with respect to Ge buffer. The solid line is the isocomposition line for the GeSn layers of each sample. The $\overline{2}24$ RSM was not measured for sample S29 annealed for 8 h since no changes in the strain state and Sn content in the GeSn layer was concluded by comparing the 004 $\omega/2\theta$ scans for sample S29 annealed for 4 and 8 h.

The samples were chosen such that:

(1) The level of strain in S14 and S15 were the same at -10×10^{-3} while the composition is 8% for sample S14 and 9% for S15. Likewise, the level of strain in both S29 and S32 were the same at -5×10^{-3}, while the composition is 9% for S29 and 10% for S32 (Figures 1 and 2). These samples allowed us to compare the effect of annealing on as-grown GeSn with the same level of strain but different Sn compositions.

(2) The composition for samples S15 and S29 is both at 9%. However, the strain in these samples is very different, with values of -10×10^{-3} for S15 and only half as much at -5×10^{-3} for S29 (Figures 1 and 2). The difference in strain is accomplished by the growth of different thicknesses. As a result, by comparing samples S15 with S29 we are comparing samples with the same % Sn composition but different levels of strain in the as-grown samples.

(3) Moreover, all four samples are chosen with a Sn concentration that places them near the indirect to direct optical transition point, where the PL sensitivity to changes in composition or strain is very high. This high sensitivity allows us to amplify the connections between strain, composition, defect density, and observed PL before and after annealing.

3. Results and Discussion

To examine these connections for our samples at elevated temperatures, we specifically investigated (1) X-ray diffraction for all samples, (2) Photoluminescence from samples with the same level of strain but different Sn composition, and (3) Photoluminescence from samples with the same Sn composition but different level of strain. All three were investigated as a function of annealing at 2, 4, and 8 h at 300 °C. X-ray diffraction measurements provided the density of misfit dislocations, composition, and level of strain. Likewise, PL measurements provided the PL intensity and the indirect and direct PL peaks as a function of annealing time. Analysis demonstrated that the (1) composition and level of strain influenced the separation between the indirect and direct optical transitions, while (2) the level of strain influenced the misfit dislocations defect density and surface roughness. It also revealed that the changes in the separation between the indirect and direct optical transitions due to annealing increased the PL emission while changes in the defect density and surface roughness decreased the PL emission. Consequently, the competition between these two factors determined the impact of annealing on the PL emission.

3.1. X-ray Diffraction Measurements

X-ray diffraction measurements were taken for samples S14, S15, S29, and S32, to resolve the internal strain, Sn composition, and defect density in the GeSn layers before and after annealing. Figure 1 shows the X-ray diffraction $\omega/2\theta$ scans for all four samples containing diffraction peaks from symmetrical (004) planes of Si, Ge, and GeSn, which are seen in the order of decreasing Bragg's angle θ. The Ge peak is right shifted with respect to the bulk position (vertical dashed line), which reveals that the Ge buffer is under ~0.2% tensile strain. This value of residual strain is typical for Ge growth on Si and is explained by the mismatch of thermal expansion coefficients between the two materials [20]. A small shift is also seen for the GeSn peaks of annealed samples, indicating the reduced vertical lattice parameter, c, of the GeSn layer after annealing. The magnitude of c is estimated from the peak positions on the $\omega/2\theta$ scans by using the Bragg's law ($2d_{004}\sin\theta = n\lambda$), where $d_{004} = c/4$ is the distance between the (004) planes, $\lambda \approx 0.15406$ nm is the wavelength of the incident X-ray beam, and n is the reflection order. The X-ray data indicates only very small changes in composition for all four samples with annealing at 300 °C, even after 8 h.

More detail on the epitaxial behavior for the four GeSn samples were determined from the X-ray diffraction reciprocal space maps (RSMs) measured around the asymmetrical $\overline{2}\overline{2}4$ reflection (Figure 2). An increase of strain relaxation in the annealed GeSn layer is concluded from the shift of the GeSn peak towards the R = 1 line on the RSM that denotes full strain relaxation. Moreover, the shift follows the isocomposition line (solid line), which is a key point - the Sn composition in the GeSn layer is not changing with the annealing. A similar trend is observed in the RSM of all four samples. An additional GeSn peak that correspond to Sn composition of about 1 at.% was seen for sample S32 annealed for 4 h, which was accompanied with the emergence of bright spots on the sample surface. The selective XRD measurements (not shown here) confirmed that the Sn content in the area not covered with the spots corresponds to the nominal value. The Sn content for the four GeSn samples was calculated by first measuring the lateral lattice parameter, a, from the position of the GeSn peak on the RSM and Equation (1).

$$|Q| = \frac{2\pi}{d_{224}} = 2\pi\sqrt{\frac{8}{a^2} + \frac{16}{c^2}} \quad (1)$$

Here, Q is the diffraction vector and d_{224} is the distance between the (224) planes in a tetragonal lattice.

For a biaxially strained GeSn layer, the Sn composition, x, and strain state were obtained according with the following equations,

$$\varepsilon_z = -2\frac{C_{12}}{C_{11}}\varepsilon_x \quad (2)$$

$$a_0 = \frac{c + 2\frac{C_{12}}{C_{11}}a}{1 - 2\frac{C_{12}}{C_{11}}} \quad (3)$$

where the elastic constants C_{12} and C_{11} and the lattice parameter a_0 of the GeSn alloy are given by linear interpolation between the parameters of Sn and Ge, such as $a_0 = xa_{Sn} + (1-x)a_{Ge}$ [21]. Using the RSM data of Figure 2 coupled with RSM modelling, the strain and defect density as a function of annealing, is computed for S14, S15, S29, and S32 in Figure 3. The simulation of RSM was performed according with the kinematic theory of X-ray diffraction as described in ref. [18]. Additionally, the structural quality of all samples is compared by measuring the full width at half-maximum (FWHM) of the GeSn (004) rocking curves (see Figure S3 and Table S1 in the Supplementary Material section).

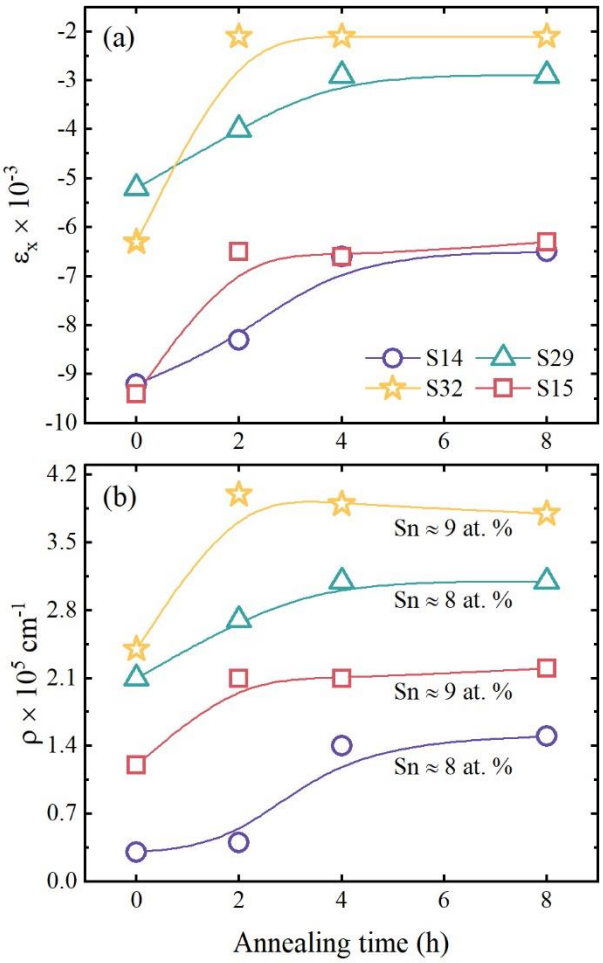

Figure 3. The strain (**a**) and density of misfit dislocations (**b**) as a function of annealing for samples S14, S15, S29, and S32.

3.2. Photoluminescence from Samples with the Same Level of Strain but Different Sn Composition

Figure 4 shows the PL spectra at 10 K for all four samples with nearly the same GeSn composition, which exhibit a totally opposite PL behavior after annealing for 2 to 8 h. There is a lot to consider when comparing the PL from different samples. For example, S14 and S15 have the same level of as-grown strain. However, the material evolution during growth is not the same. Sample S15 has more Sn added and therefore a higher level of strain during growth and a higher level of relaxation by the end of growth, at which time both S14 and S15 are at the same level of strain. This means our first expectation is that S15 has more dislocation defects than S14 in the as-grown sample which is consistent with the results in Figure 3. The second is that the competition between indirect and direct optical transitions,

as measured by the energy separation between them (ΔE), is also different with an expected smaller energy difference for S15 due to the higher Sn content. The competition between these two factors, the former tending to decrease the PL and the latter to increase the PL, can determine the corresponding behavior of the PL intensity as a function of annealing time. It is important to note here that unlike changes in the defect density, the effect of changes in ΔE is extremely nonlinear when close to the indirect to direct transition point, as is the case here.

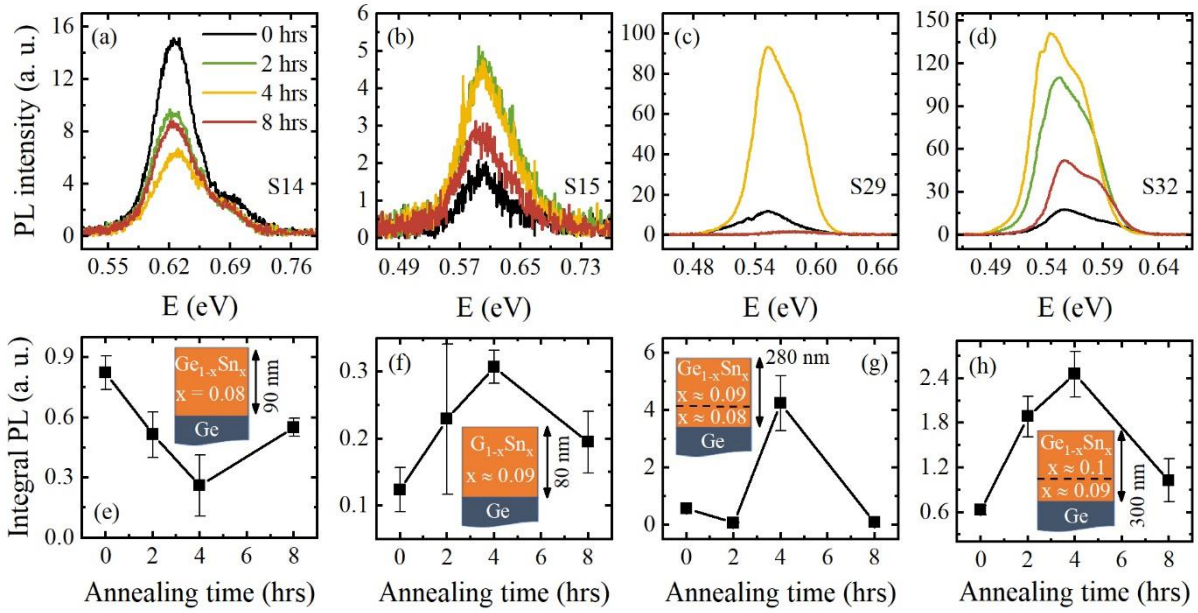

Figure 4. (**a**–**d**) PL at 10 K for four GeSn samples: S15 and S29 with about 9% Sn, S14 at 8% Sn, and S32 with about 10% Sn, and the corresponding (**e**–**h**) integrated PL. Measurements are for 0, 2, 4, and 8 h annealing. Insets indicate the GeSn structure.

Added to defect density and ΔE are optical losses due to changes in surface roughness. For example, using atomic force microscopy (AFM), the root-mean-square roughness (RMS) for all four as-grown samples is at about 0.8 nm, with only a small change to about 0.9 nm with annealing up to 4 h. However, the surfaces are noticeably rougher at about 1.7 nm, with the order of one-micron lateral size variations, after 8 h. As a result, we can expect little change in optical scattering losses at the surface up to 4 h due to annealing, but we may expect the increase in surface roughness after 8 h to introduce some added losses due to optical scattering. Consequently, we must consider three factors to play a role when comparing the effect of annealing on the PL from different samples: (1) ΔE, (2), defect density and (3) surface roughness. The AFM images for samples S14, S15, S29, and S32 annealed for 0, 4, and 8 h are shown in Figure S4 of the supplement material section.

For example, for S14, the integrated PL decreases with annealing because the increase in defect density for 2 h and 4 h has a bigger impact then ΔE. However, as we see from X-ray diffraction, the change in defect density for S14 is leveling-off after 4 h and further nonlinear changes in ΔE causes the PL to slightly increase at 8 h. Meanwhile for S15, the integrated intensity is lower than S14 when comparing the as-grown samples, due to the higher defect density. However, ΔE is smaller due to the higher Sn content making the PL more sensitive to changes in ΔE than in S14. As a result, the PL intensity increases with annealing. However, the change in strain levels-off again in 4 h, so that the PL intensity falls after 4 h, perhaps due to increased surface scattering losses related to the increase of surface roughness from 0.9 nm at 4 h to 2.1 nm at 8 h. The point being that X-ray diffraction and AFM data can provide the change in the level of strain, composition, defect density, and surface roughness to explain the behavior of annealing at 300 °C on the PL emission.

Of course, this comparison can be less speculative and more quantitative with knowledge of the behavior of ΔE, which we must investigated.

For S29 and S32, we again have equal levels of strain but different Sn content. However, the outcome is a bit different since both have a higher level of Sn content than either S14 or S15. This means that ΔE is smaller for S29 and even smaller for S32. As a result, the PL for S29 and S32 increases with annealing until 4 h when no further strain relaxation is observed, and an increase in surface roughness and optical scattering can reduce the collected PL.

3.3. Photoluminescence from Samples with the Same Sn Composition but Different Level of Strain and Measurement of ΔE

From the X-ray diffraction data and analysis for samples S14 to S32, we observe an increasing Sn content and level of defect density. However, the PL sensitivity to ΔE, and the impact of small changes in ΔE, increase more strongly as the transition point is approached. As already noted, to examine this more closely, an investigation of ΔE for samples S14 to S32 is required. To accomplish this, the idea is to deconvolve the PL into two Gaussian peaks, the indirect optical transition, and the direct optical transition. This would allow us to (1) calculate ΔE for S14 and S32 and (2) use a comparison of the ratio of the intensity of the PL of the higher energy peak to the lower energy peak as a function of temperature to identify which of the two peaks is the direct transition. For example, if the higher energy is the direct optical transition, the PL ratio will increase with temperature as carriers are transferred from the indirect valley to the direct valley reaching a new equilibrium.

Based on this idea, the measured PL spectra for samples S14 and S32 were taken using both 532 nm and 1064 nm wavelengths. Figure 5 shows the PL result for sample S14 that used the 1064 nm laser wavelength for excitation to probe the entire GeSn layer, while the PL for S32 is shown using the 532 nm laser excitation to limit the excitation to the top layer. For 532 nm incident light, the absorption coefficient in Ge is 5.58×10^5 cm^{-1} so that the intensity of light drops to 36% at about 18 nm below the sample surface [19]. This allows us to neglect the contribution from the bottom GeSn layer in sample S32 in the collected PL. However, the same trend in PL was observed using either wavelength although a higher PL intensity was always observed using 532 nm. For both samples, two peaks represented by two distinct Gaussian functions were deconvolved and are an excellent fit to the PL spectra. The high and low energy peaks were initially assumed as the indirect (L^{HH}) and direct (Γ^{HH}) interband transitions, respectively but will be confirmed later. An analysis of the X-ray diffraction data indicates that the change of the positions of the L^{HH} and Γ^{HH} peaks for the two samples with annealing is dominantly caused by changes in the level of strain in the annealed GeSn layers as opposed to changes in the Sn content which remained relatively constant.

The behavior of the integrated PL is also of interest and shown in the insert of Figure 5b. For example, for S32 the behavior of the integrated PL is very dramatic and can be understood by examining the separation between the peak energy for the L^{HH} valley transition and the Γ^{HH} valley transition, or $\Delta E = L^{HH} - \Gamma^{HH}$. Figure 6a shows the decrease of ΔE with annealing time owing to the compressive strain relaxation in the GeSn layer [22]. We observe that ΔE is significantly smaller by 27 ± 2 meV for sample S32 compared to S14 due to the higher Sn content. As a result, the PL from S32 has a larger direct bandgap component Γ^{HH} as compared to that of sample S14. This is expected due to the PL non-linear dependence on ΔE resulting in more efficient light emission [23]. The increase of the Γ valley population is confirmed in Figure 6b, which shows that the peak height ratio Γ^{HH}/L^{HH} increases dramatically with decreasing ΔE. The increased emission from the Γ^{HH} valley for sample S32 is also in good agreement with the enhanced integrated PL in Figure 5b.

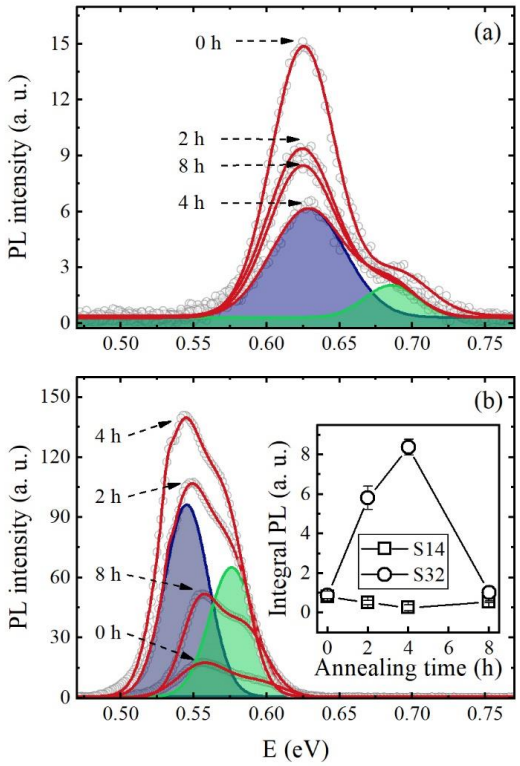

Figure 5. PL spectra of sample S14 (**a**), S32 (**b**) measured at 10 K before and after annealing. Inset shows the integrated PL as a function of annealing time.

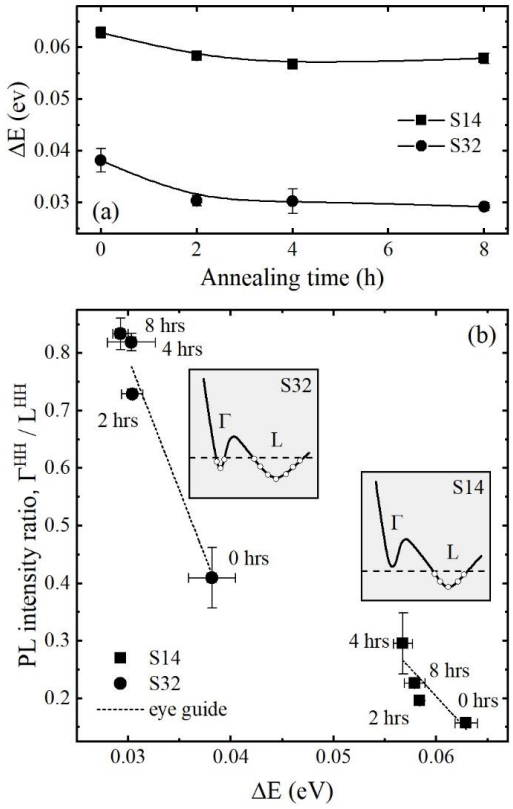

Figure 6. (**a**) The energy separation between Γ^{HH} and L^{HH} peaks on the measured PL and (**b**) the Γ^{HH}/L^{HH} intensity ratio.

To confirm our understanding, temperature dependent PL measurements were performed to examine the relative peak intensity of direct (Γ^{HH}) and indirect (L^{HH}) transitions as a function of temperature (Figure 7). A red shift of both Γ^{HH} and L^{HH} peaks is seen with increasing temperature, which agrees with the bandgap shrinkage [24,25]. The peak intensities and their positions were determined again by fitting each measured spectrum with two Gaussian functions. However, due to the reduced PL intensity with increasing temperature, the Γ^{HH} and L^{HH} peaks were not resolved on the spectra measured above 200 K.

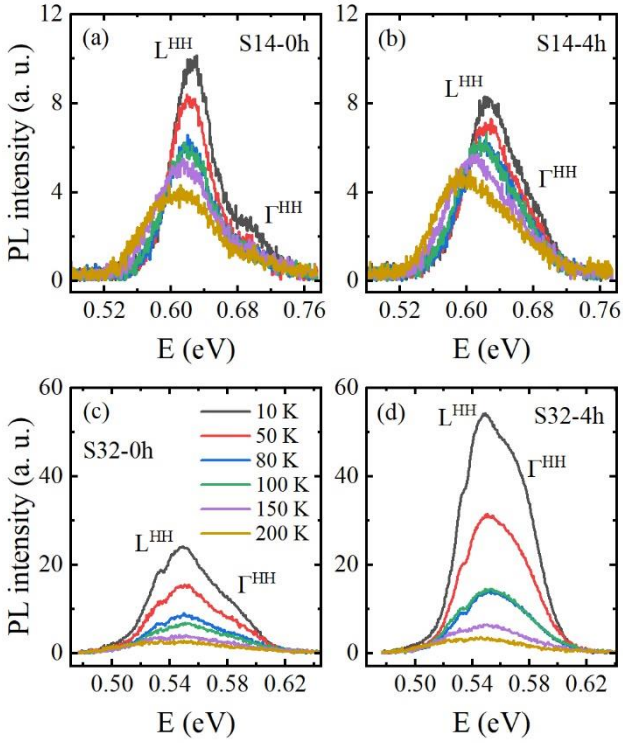

Figure 7. The temperature dependent PL from the GeSn layer of samples S14 and S32. (**a**) S14-0 h; (**b**) S14-4 h; (**c**) S32-0 h; (**d**) S32-4 h.

The increase of peak intensity ratio Γ^{HH}/L^{HH} with temperature is shown in Figure 8. This indicates that the assumption that the peak Γ^{HH} located at the higher energies on the PL spectra indeed corresponds to direct transitions and that although ΔE follows a decreasing trend from sample S14 to S32, it had not gone through zero and become negative.

Finally based on our understanding gained from investigating the PL from samples S14 to S32, we examined a fifth sample, S45, which has a higher Sn content of 12% but is fully strained (Figure S1). This is a result of the fact that the sample thickness is only 45 nm and well below the critical thickness for strain relaxation [26–28]. As a result, the as-grown samples have a much higher level of strain and a corresponding lower density of misfit/threading dislocations when compared to structures S14 and S32. The density of misfit dislocations is in fact near zero for the as-grown S45 sample and remains zero after 2 h of annealing at 300 °C. However, it then increases to 0.5×10^5 cm^{-1} after 2.5 h, and 1.0×10^5 cm^{-1} after for 4 h, due to strain relaxation. Meanwhile the strain is -15×10^{-3} in the as-grown sample and does not relax after 2 h but does relax by 2.5 h and after 4 h. Sample S45 also corresponds nicely with that used in a previous comprehensive study of optical transitions in a specific direct-bandgap $Ge_{0.875}Sn_{0.125}$ alloy via photoluminescence (PL) measurements [17]. Based on results from this previous work, our sample S45 at a strain level of -15×10^{-3}, is solidly indirect with little, if any, role expected from the direct transition, despite the high Sn content.

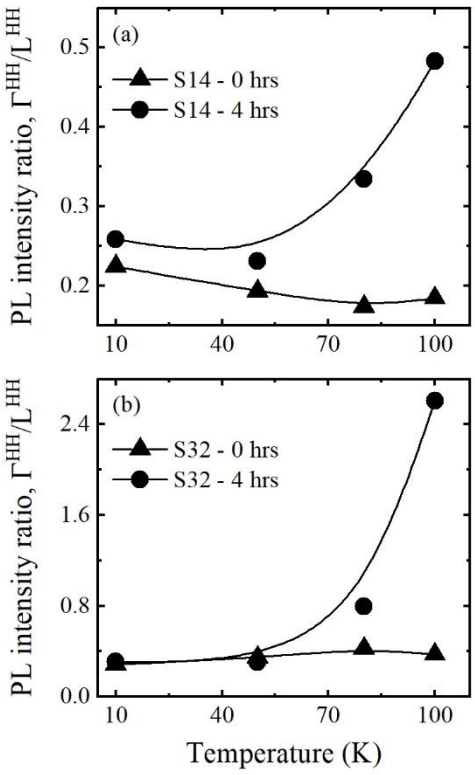

Figure 8. Temperature dependent PL intensity ratio Γ^{HH}/L^{HH}. (**a**) S14; (**b**) S32.

Meanwhile, the PL from S45 is shown in Figure S2 and indicates two transitions **of** comparative heights and a large ΔE of about 120 meV. However, in this case we can conclude that the transitions represent the L^{HH} and L^{HL} transitions, not L^{HH} and Γ^{HH}. In this case we can expected a ΔE of about 120 meV at a strain level of -15×10^{-3} as indicated in Figure 1 of reference [17]. Analysis of S45 at least suggests that relaxation of high stress GeSn is best to occur during growth when the segregated Sn can be incorporated into the growth.

4. Conclusions

In conclusion, we have examined the connection between strain, composition, defect density and the PL observed before and after annealing at 300 °C for GeSn samples with Sn content of 8% to 10% near the indirect to direct transition point. Our results show that for samples with a composition near the transition point, the composition and level of strain both influenced ΔE, the separation between the indirect and direct optical transitions, while changes in the level of strain also influenced the misfit dislocations defect density and surface roughness. The effect of annealing is to lower the level of strain, decreasing ΔE, which in-turn, due to the competition between indirect and direct optical transitions, increases the PL emission. By lowering the level of strain, annealing also simultaneously increases the defect density and surface roughness, both of which decreases the PL emission. Consequently, the competition between these factors, ΔE and the change in defect density and surface roughness, determines the impact of annealing on the PL emission. As a result, annealing can both increase and decrease the collected PL depending on how close the sample is to the indirect to direct transition point. This is because the dependence on ΔE is extremely nonlinear for compositions near the transition. That is, the same change in ΔE can have a small or a large effect, depending on the relative location to the transition point. Of course, above the transition point the PL simply behaves as a direct bandgap semiconductor.

These results suggest that capping GeSn samples with Ge could reduce the effect of surface roughness and result in improved performance when operated above room temperature.

Supplementary Materials: The following are available online at https://www.mdpi.com/article/10.3390/cryst11080905/s1, X-ray diffraction and temperature-dependent photoluminescence data for sample.

Author Contributions: Conceptualization, G.S., S.-Q.Y., H.S. and O.O., methodology, H.S. and O.O.; validation, H.S. and O.O.; formal analysis, S.-Q.Y., G.S., H.S., A.K., Y.I.M. and O.O.; investigation, O.O. and H.S.; resources, G.S. and S.-Q.Y.; curation, O.O., A.S., K.P., S.O., A.K. and H.S.; writing—original draft preparation, S.-Q.Y., G.S., H.S., and O.O.; growth, J.M. and J.T.; supervision, G.S. and S.-Q.Y.; project administration, S.-Q.Y.; funding acquisition, S.-Q.Y. and G.S. All authors have read and agreed to the published version of the manuscript.

Funding: This work was supported by the Multidisciplinary University Research Initiative (MURI) Program through U.S. Air Force Office of Scientific Research (AFOSR) Grant No. FA9550-19-1-0341.

Conflicts of Interest: The authors declare no conflict of interest.

References

1. Soref, R.A. Silicon-Based Optoelectronics. *Proc. IEEE* **1993**, *81*, 1687–1706. [CrossRef]
2. Soref, R.A.; Friedman, L. Direct-Gap Ge/GeSn/Si and GeSn/Ge/Si Heterostructures. *Superlattices Microstruct.* **1993**, *14*, 189–193. [CrossRef]
3. Tseng, H.H.; Wu, K.Y.; Li, H.; Mashanov, V.; Cheng, H.H.; Sun, G.; Soref, R.A. Mid-Infrared Electroluminescence from a $Ge/Ge_{0.922}Sn_{0.078}/Ge$ Double Heterostructure p-i-n Diode on a Si Substrate. *Appl. Phys. Lett.* **2013**, *102*, 182106. [CrossRef]
4. Homewood, K.P.; Lourenço, M.A. The Rise of the GeSn Laser. *Nat. Photonics* **2015**, *9*, 78–79. [CrossRef]
5. Oehme, M.; Kostecki, K.; Schmid, M.; Oliveira, F.; Kasper, E.; Schulze, J. Epitaxial Growth of Strained and Unstrained GeSn Alloys up to 25% Sn. *Thin Solid Films* **2014**, *557*, 169–172. [CrossRef]
6. Du, W.; Zhou, Y.; Ghetmiri, S.A.; Mosleh, A.; Conley, B.R.; Nazzal, A.; Soref, R.A.; Sun, G.; Tolle, J.; Margetis, J.; et al. Room-Temperature Electroluminescence from $Ge/Ge_{1-X}Sn_x/Ge$ Diodes on Si Substrates. *Appl. Phys. Lett.* **2014**, *104*, 241110. [CrossRef]
7. Tseng, H.H.; Li, H.; Mashanov, V.; Yang, Y.J.; Cheng, H.H.; Chang, G.E.; Soref, R.A.; Sun, G. GeSn-Based p-i-n Photodiodes with Strained Active Layer on a Si Wafer. *Appl. Phys. Lett.* **2013**, *103*, 231907. [CrossRef]
8. Alberi, K.; Blacksberg, J.; Bell, L.D.; Nikzad, S.; Yu, K.M.; Dubon, O.D.; Walukiewicz, W. Band Anticrossing in Highly Mismatched Sn_xGe_{1-x} Semiconducting Alloys. *Phys. Rev. B* **2008**, *77*, 073202. [CrossRef]
9. Kondratenko, S.V.; Hyrka, Y.V.; Mazur, Y.I.; Kuchuk, A.V.; Dou, W.; Tran, H.; Margetis, J.; Tolle, J.; Yu, S.-Q.; Salamo, G.J. Photovoltage Spectroscopy of Direct and Indirect Bandgaps of Strained Ge1-XSnx Thin Films on a Ge/Si(001) Substrate. *Acta Mater.* **2019**, *171*, 40–47. [CrossRef]
10. Ghetmiri, S.A.; Du, W.; Conley, B.R.; Mosleh, A.; Nazzal, A.; Sun, G.; Soref, R.A.; Margetis, J.; Tolle, J.; Naseem, H.A.; et al. Shortwave-Infrared Photoluminescence from $Ge_{1-x}Sn_x$ Thin Films on Silicon. *J. Vac. Sci. Technol. B* **2014**, *32*, 060601. [CrossRef]
11. Tonkikh, A.A.; Zakharov, N.D.; Suvorova, A.A.; Eisenschmidt, C.; Schilling, J.; Werner, P. Cubic Phase Sn-Rich GeSn Nanocrystals in a Ge Matrix. *Cryst. Growth Des.* **2014**, *14*, 1617–1622. [CrossRef]
12. Wirths, S.; Buca, D.; Ikonic, Z.; Harrison, P.; Tiedemann, A.T.; Holländer, B.; Stoica, T.; Mussler, G.; Breuer, U.; Hartmann, J.M.; et al. SiGeSn Growth Studies Using Reduced Pressure Chemical Vapor Deposition towards Optoelectronic Applications. *Thin Solid Film.* **2014**, *557*, 183–187. [CrossRef]
13. Senaratne, C.L.; Gallagher, J.D.; Aoki, T.; Kouvetakis, J.; Menéndez, J. Advances in Light Emission from Group-IV Alloys via Lattice Engineering and n-Type Doping Based on Custom-Designed Chemistries. *Chem. Mater.* **2014**, *26*, 6033–6041. [CrossRef]
14. Mosleh, A.; Alher, M.; Cousar, L.C.; Du, W.; Ghetmiri, S.A.; Al-Kabi, S.; Dou, W.; Grant, P.C.; Sun, G.; Soref, R.A.; et al. Buffer-Free GeSn and SiGeSn Growth on Si Substrate Using In Situ SnD4 Gas Mixing. *J. Electron. Mater.* **2016**, *45*, 2051–2058. [CrossRef]
15. Du, W.; Ghetmiri, S.A.; Conley, B.R.; Mosleh, A.; Nazzal, A.; Soref, R.A.; Sun, G.; Tolle, J.; Margetis, J.; Naseem, H.A.; et al. Competition of Optical Transitions between Direct and Indirect Bandgaps in $Ge_{1-x}Sn_x$. *Appl. Phys. Lett.* **2014**, *105*, 051104. [CrossRef]
16. Harris, T.R.; Ryu, M.-Y.; Yeo, Y.K.; Wang, B.; Senaratne, C.L.; Kouvetakis, J. Direct Bandgap Cross-over Point of Ge1-YSny Grown on Si Estimated through Temperature-Dependent Photoluminescence Studies. *J. Appl. Phys.* **2016**, *120*, 085706. [CrossRef]
17. Stange, D.; Wirths, S.; von den Driesch, N.; Mussler, G.; Stoica, T.; Ikonic, Z.; Hartmann, J.M.; Mantl, S.; Grützmacher, D.; Buca, D. Optical Transitions in Direct-Bandgap Ge_{1-x} Sn_x Alloys. *ACS Photonics* **2015**, *2*, 1539–1545. [CrossRef]
18. Stanchu, H.V.; Kuchuk, A.V.; Mazur, Y.I.; Pandey, K.; de Oliveira, F.M.; Benamara, M.; Teodoro, M.D.; Yu, S.-Q.; Salamo, G.J. Quantitative Correlation Study of Dislocation Generation, Strain Relief, and Sn Outdiffusion in Thermally Annealed GeSn Epilayers. *Cryst. Growth Des.* **2021**, *21*, 1666–1673. [CrossRef]

19. Du, W.; Ghetmiri, S.A.; Margetis, J.; Al-Kabi, S.; Zhou, Y.; Liu, J.; Sun, G.; Soref, R.A.; Tolle, J.; Li, B.; et al. Investigation of Optical Transitions in a SiGeSn/GeSn/SiGeSn Single Quantum Well Structure. *J. Appl. Phys.* **2017**, *122*, 123102. [CrossRef]
20. Cannon, D.D.; Liu, J.; Ishikawa, Y.; Wada, K.; Danielson, D.T.; Jongthammanurak, S.; Michel, J.; Kimerling, L.C. Tensile Strained Epitaxial Ge Films on Si(100) Substrates with Potential Application in L-Band Telecommunications. *Appl. Phys. Lett.* **2004**, *84*, 906–908. [CrossRef]
21. Stanchu, H.; Kuchuk, A.V.; Mazur, Y.I.; Margetis, J.; Tolle, J.; Richter, J.; Yu, S.-Q.; Salamo, G.J. X-Ray Diffraction Study of Strain Relaxation, Spontaneous Compositional Gradient, and Dislocation Density in GeSn/Ge/Si(100) Heterostructures. *Semicond. Sci. Technol.* **2020**, *35*, 075009. [CrossRef]
22. De Kersauson, M.; Jakomin, R.; El Kurdi, M.; Beaudoin, G.; Zerounian, N.; Aniel, F.; Sauvage, S.; Sagnes, I.; Boucaud, P. Direct and Indirect Band Gap Room Temperature Electroluminescence of Ge Diodes. *J. Appl. Phys.* **2010**, *108*, 023105. [CrossRef]
23. Sun, X.; Liu, J.; Kimerling, L.C.; Michel, J. Direct Gap Photoluminescence of n -Type Tensile-Strained Ge-on-Si. *Appl. Phys. Lett.* **2009**, *95*, 011911. [CrossRef]
24. Pezzoli, F.; Giorgioni, A.; Patchett, D.; Myronov, M. Temperature-Dependent Photoluminescence Characteristics of GeSn Epitaxial Layers. *ACS Photonics* **2016**, *3*, 2004–2009. [CrossRef]
25. Zelazna, K.; Wełna, M.; Misiewicz, J.; Dekoster, J.; Kudrawiec, R. Temperature Dependence of Energy Gap of $Ge_{1-x}Sn_x$ Alloys with x < 0.11 Studied by Photoreflectance. *J. Phys. D Appl. Phys.* **2016**, *49*, 235301. [CrossRef]
26. Matthews, J.W.; Blakeslee, A.E. Defects in Epitaxial Multilayers. I. Misfit Dislocations. *J. Cryst. Growth* **1974**, *27*, 118–125. [CrossRef]
27. Wang, W.; Zhou, Q.; Dong, Y.; Tok, E.S.; Yeo, Y.-C. Critical Thickness for Strain Relaxation of $Ge_1 - xSn_x$ ($x \leq 0.17$) Grown by Molecular Beam Epitaxy on Ge(001). *Appl. Phys. Lett.* **2015**, *106*, 232106. [CrossRef]
28. People, R.; Bean, J.C. Calculation of Critical Layer Thickness versus Lattice Mismatch for GexSi1−x/Si Strained-layer Heterostructures. *Appl. Phys. Lett.* **1985**, *47*, 322–324. [CrossRef]